Medical Image Analysis 55 (2019) 41–48

Contents lists available at ScienceDirect

Medical Image Analysis

journal homepage: www.elsevier.com/locate/media

A kernel-based image denoising method for improving parametric image generation

Hsuan-Ming Huang[a,*], Chieh Lin[b]

[a] Institute of Medical Device and Imaging, College of Medicine, National Taiwan University, No.1, Sec. 1, Jen Ai Rd., Zhongzheng Dist., Taipei City 100, Taiwan
[b] Department of Nuclear Medicine, Chang Gung Memorial Hospital, No. 5 Fu-Shin Street, Kwei-Shan, Taoyuan County, Taiwan

ARTICLE INFO

Article history:
Received 26 September 2018
Revised 20 February 2019
Accepted 13 April 2019
Available online 17 April 2019

Keywords:
Kernel method
Total difference
General threshold filtering
Intra-voxel incoherent motion
Diffusion-weighted imaging

ABSTRACT

One of the main challenges in the pixel-wise modeling analysis is the presence of high noise levels. Wang and Qi proposed a kernel-based method for dynamic positron emission tomgraphy reconstruction. Inspired by this method, we propose a kernel-based image denoising method based on the minimization of a kernel-based lp-norm regularized problem. To solve the kernel-based image denoising problem, we used the general-threshold filtering algorithm in combination with total difference. In the present study, we investigated whether diffusion-weighted magnetic resonance imaging (DW-MRI) data denoised using the proposed method can provide improved intravoxel incoherent motion (IVIM) parametric images. We also compared the proposed method with the method using the local principal component analysis (LPCA). The simulated DW-MR magnitude images are assumed to have Rician distributed noise. Computer simulations show that the proposed image denoising method can achieve a better bias-variance trade-off than the LPCA method. Moreover, the proposed method can reduce variance while simultaneously preserving edges in the parametric images. We tested our image denoising method on in vivo DW-MRI data, and the result showed that the denoised DWI-MRI data obtained using the proposed method can substantially improve the quality of IVIM parametric images.

1. Introduction

Over the last two decades, the quantitative analysis of medical imaging data has become increasingly important in both preclinical and clinical studies. Many previous studies have shown that the quantitative analysis of dynamic data such as positron emission tomography (PET) (Muzi et al., 2012), perfusion computed tomography (CT) (Valdiviezo et al., 2010), contrast- enhanced magnetic resonance imaging (MRI) (Khalifa et al., 2014) and diffusion-weighted (DW) MRI (Koh et al., 2011), can improve the diagnosis of disease, the prediction of response to treatment, and the monitoring of progression of disease. Traditionally, model parameters are estimated using data obtained from a region of interest (ROI). In contrast, one can generate the parametric image of each model parameter through pixel-wise parameter estimation. Compared with the ROI-based analysis, the pixel-wise modeling analysis can provide more useful and important information because it can reveal status of each individual pixel. However, due to the fact that the noise level in the individual pixel is high, parametric images often suffer from poor image quality.

In order to improve the quality of parametric images, many different approaches have been proposed. For example, parametric images can be improved by using direction reconstruction of kinetic parameter images (Wang and Qi, 2009), advanced iterative image reconstruction algorithms (Fessler, 2010; Geyer et al., 2015; Tong et al., 2010) and advanced curve fitting algorithms (Freiman et al., 2013; Guo et al., 2009; Kayal et al., 2017; Lin et al., 2017; Orton et al., 2014). It has been shown that using either direct reconstruction or advanced iterative image reconstruction algorithms could provide improved parametric images (Wang and Qi, 2009), but these methods are not supplied by the vendor. It was reported that parametric images obtained using advanced curve fitting algorithms such as Bayesian probability methods (Freiman et al., 2013; Orton et al., 2014) and total-variation (TV) based methods (Guo et al., 2009; Kayal et al., 2017; Lin et al., 2017) had better bias-variance characteristics than those obtained from conventional curve fitting algorithms such as Levenberg–Marquardt algorithm (Levenberg, 1944; Marquardt, 1963) and trust-region-reflective algorithm (Branch et al., 1999; Byrd et al., 1988). However, advanced curve fitting algorithms generally take long time to estimate the parameters.

Compared to the above-mentioned approaches, denoising imaging data seems to be a better way to improve the quality of parametric images. First, imaging data are stored in common image

* Corresponding author.
E-mail address: b9003205@gmail.com (H.-M. Huang).

https://doi.org/10.1016/j.media.2019.04.003
1361-8415/

file formats (e.g., DICOM, NIfTI, Interfile, ECAT), and many software tools provide easy access to such data. Second, many computationally fast image denoising methods have been proposed (Manjón et al., 2013; Reischauer and Gutzeit, 2017). In addition, one can use multi-core processor and graphics processing unit to further reduce the computation time. Third, several robust image denoising methods have been proposed (Bian et al., 2014; Dutta et al., 2013; Manjón et al., 2013; Reischauer and Gutzeit, 2017). Although most image denoising algorithms have several algorithm parameters, some parameters (e.g., noise levels) can be determined automatically. Nevertheless, the smoothing parameter should be carefully chosen. Excessive smoothing can reduce the variance of parameter estimates but at the risk of increasing bias. In addition, excessive smoothing can result in oversmoothing of edge and loss of detail.

Our previous study showed that the total difference-based general threshold filtering (TD-GTF) algorithm can reduce noise in DW-MRI data and provide improved parametric images (Lin et al., 2018). In particular, the proposed TD-GTF method has good edge preserving capability. However, few model parameters (e.g., pseudodiffusion coefficient) are still difficult to estimate. Recently, a kernel method has been proposed for dynamic PET reconstruction (Wang and Qi, 2015) and extended to direct reconstruction of Patlak parametric images (Gong et al., 2018). In this study, we apply the kernel-based method (Wang and Qi, 2015) to the problem of image denoising and propose a new image denoising method that combines the kernel-based method (Wang and Qi, 2015) with the TD-GTF algorithm (Lin et al., 2018). We investigate whether the proposed method can improve intravoxel incoherent motion (IVIM) (LeBihan et al., 1988, 1986) parametric images derived from denoised DW-MRI data.

This paper is organized as follows. In Section 2, we will describe the proposed image denoising method. In Section 3, we will describe the IVIM analysis and the setup for our simulation and experimental studies. We will simulate DW-MR magnitude images which are generally assumed to follow a Rician distribution (Gudbjartsson et al., 1995; Sijbers et al., 1998). In Section 4, we will present computer simulation and experimental results. Finally, in Section 5, we will discuss some related issues and state our conclusions.

2. Materials and methods

2.1. Kernel-based approach for image denoising

Based on the kernel methods used in image reconstruction, the kernel representation for the image intensity at pixel j (f_j) can be written as (Wang and Qi, 2015):

$$f_j = \sum_{l=1}^{N} k(F_j, F_l)\alpha_l \tag{1}$$

where N is the total number of pixels in the image, $k(F_j, F_l)$ is a positive definite kernel (Hofmann et al., 2008) obtained from prior information (Wang and Qi, 2015), F_j and F_l are feature vectors for pixels j and l, respectively, and α_l is the unknown coefficient image to be recovered. In this study, we used the radial Gaussian kernel (Schölkopf and Smola, 2001; Wang and Qi, 2015).

$$k(F_j, F_l) = \exp\left(-\frac{\left\|F_j - F_l\right\|^2}{2\sigma^2}\right) \tag{2}$$

where σ is a kernel parameter. The matrix-vector form of Eq. (1) is $f = K\alpha$. The column vectors of the kernel matrix K can be viewed as a basis function for image representation, and the (j,l)th element of the kernel matrix K can be expressed as:

$$K_{j,l} = \begin{cases} k(F_j, F_l) & F_l \in \text{knn of } F_j \\ 0 & \text{otherwise} \end{cases} \tag{3}$$

To reduce the computational time, we performed a k-nearest neighbor (knn) search using the Euclidean distance between F_j and F_l (Wang and Qi, 2015).

The kernelized image denoising problem can be solved by considering the following lp-norm ($0 \le p \le 1$) regularization based problem (Miao and Yu, 2015; Yu and Wang, 2010):

$$\min_{\alpha}\left\{\|g - K\alpha\|^2 + \lambda\|\Phi f\|_p^p\right\} \tag{4}$$

where g is the noisy image, λ is a regularization parameter providing the tradeoff between the least square term and the penalty term, and Φ is the sparse transform (e.g., TV and TD). The sparse transform used in this study was TD (Yu and Wang, 2010).

$$\Phi f = \sum_{x=1}^{X}\sum_{y=1}^{Y}\left|f_{x,y} - f_{x+1,y}\right| + \left|f_{x,y} - f_{x,y+1}\right| \tag{5}$$

where x and y denote the two-dimensional location of a pixel and XY = N. Based on the GTF algorithm (Miao and Yu, 2015; Yu and Wang, 2010), we can construct a pseudo-inverse of the TD, and the minimization problem in Eq. (4) can be recursively solved by the following two equations:

$$\alpha^n = \alpha^{n-1} + K^T\left(g - K\alpha^{n-1}\right) \tag{6}$$

$$\begin{aligned}\tilde{f}^n_{x,y} = \frac{1}{4}\Big[&q\left(f^n_{x,y}, f^n_{x+1,y}, \omega_{\lambda,p}\right) + q\left(f^n_{x,y}, f^n_{x,y+1}, \omega_{\lambda,p}\right)\\ &+ q\left(f^n_{x,y}, f^n_{x-1,y}, \omega_{\lambda,p}\right) + q\left(f^n_{x,y}, f^n_{x,y-1}, \omega_{\lambda,p}\right)\Big]\end{aligned} \tag{7}$$

and

$$q(a, b, \omega_{\lambda,p}) = \begin{cases} (a+b)/2 & \text{if } |a-b| < \omega_{\lambda,p} \\ a - \text{sgn}(a-b)\times h_{\lambda,p}(a,b)/2 & \text{if } |a-b| \ge \omega_{\lambda,p} \end{cases} \tag{8}$$

where $f^n = K\alpha^n$, the superscript "T" denotes matrix transpose, n is the iteration number, $\omega_{\lambda,p} = 0.5\times(2-pp)\times pp$, $pp = [(1-p)^{(p-1)/(2-p)}]\times[\lambda^{1/(2-p)}]$ and $h_{\lambda,p}(a, b)$ is an approximate analytic thresholding function which can be expressed as follows (Miao and Yu, 2015):

$$\begin{aligned}h_{\lambda,p}(a,b) = 0.5\times\lambda\times p\times\{&|a-b| - 0.5\times\lambda\times p\times[|a-b|\\ &- 0.5\times p\times pp]^{p-1}\}^{p-1}\end{aligned} \tag{9}$$

For more details on the construction of the GTF-based pseudo-inverse of the TD, we refer interested readers to (Miao and Yu, 2015; Yu and Wang, 2010). The proposed image denoising algorithm can be summarized by the following pseudo-code:

1: Set p = 0.7, α^0=0, and g (i.e. the singe b-value noisy DW-MRI data);
2: Set λ (i.e. the pre-estimated noise) and K (i.e. the pre-calculated kernel matrix);
3: for n = 1:10
4: $\alpha^n = \alpha^{n-1} + K^T(g - K\alpha^{n-1})$; // Eq. (6)
5: $f^n = K\alpha^n$;
6: for r = 1:5
7: $\tilde{f}^n$ =TD-GTF(f^n, λ, p); // Eqs. (7)–(9)
8: $f^n = \tilde{f}^n$;
9: end for r
10: $\alpha^n = K^T\tilde{f}^n$;
11: end for n
12: $\hat{f} = K\alpha^n$; // $\hat{f}$ is the final denoised DW-MRI data.

The proposed method, like most image denoising methods, has several algorithm parameters. First, we repeated the TD-GTF

method five times (i.e. lines 6–9). This thresholding process is repeated several times to provide sufficient noise reduction. Second, the parameter p was set to 0.7 which should provide adequate edge-preserving noise suppression (Lin et al., 2018). Third, the number of iterations was set to 10 (i.e. $n = 10$) simply because the proposed method could rapidly achieve stable results (see Fig. A1). The regularization parameter (λ) determines the threshold value ($\omega_{\lambda,\,p}$) for a given p value. A larger λ generates a larger $\omega_{\lambda,\,p}$ and gives a sparer solution (Miao and Yu, 2015). In this study, λ was set to the Rician noise averaged over all b-value DW-MRI data. Here, we used the median absolute deviation estimator (Coupé et al., 2010) to estimate the Rician noise of each b-value DW-MRI data.

In addition to the above-mentioned parameters, kernel matrix construction and kernel parameter selection are important. To denoise DW-MRI data using the proposed method, feature sets (i.e. prior images) used to construct the kernel matrix are required. For the proposed kernel method, a series of DW-MRI data acquired with 9 b-values (i.e. $b \neq 0$) were used to form the feature sets $\{F_j\}_{j=1}^{N}$.

$$F_j = \left[f_{j,1},\ f_{j,2}, f_{j,3}\right]^T \tag{10}$$

where $f_{j,1}$, $f_{j,2}$ and $f_{j,3}$ are the summed image intensity values at pixel j, obtained from $[S(b_2) + S(b_3) + S(b_4)]$, $[S(b_5) + S(b_6) + S(b_7)]$ and $[S(b_8) + S(b_9) + S(b_{10})]$, respectively. $S(b_i)$ denotes the noisy DW-MRI signal intensity obtained by the ith b value. In order to reduce the computation time, knn search was performed in a 7×7 window for each pixel in the prior images. The number of neighbors was 48, and the σ value of the radial Gaussian kernel function was set to 1. Like what they did in (Wang and Qi, 2015), the feature points (f_j) were normalized by its standard deviation (SD).

$$\bar{f}_{j,m} = f_{j,m}/\sigma_m(f) \tag{11}$$

where $\sigma_m(f)$ is the SD of the mth element of f_j ($m = 1, 2, 3$) over all of the pixels. Finally, the kernel matrix K was calculated using $\bar{f}_{j,m}$ by Eq. (3). To improve the quality of the kernel matrix K, the kernel matrix K was symmetrized using $\mathrm{diag}^{-1}[K1_N]K$ (Milanfar, 2013; Wang and Qi, 2015). 1N denotes the $N \times 1$ vector of ones and $\mathrm{diag}^{-1}[a]$ denotes the diagonalization of the matrix 1/a.

It is important to note that feature points (f_j) obtained from noisy DW-MRI data are not good when DW-MRI data have a low signal-to-noise ratio (SNR). To provide better prior images for constructing the kernel matrix, the smoothed DW-MRI data were used. We found that the noisy DW-MRI data filtered by the linear minimum mean square error (LMMSE) estimator (Aja-Fernandez et al., 2008) and the local principal component analysis (LPCA) method (Manjón et al., 2013) can provide good prior images. As a result, the new feature sets $\{F_j\}_{j=1}^{N}$ are

$$F_j = \left[f_{j,1}^{LMMSE}, f_{j,2}^{LMMSE}, f_{j,3}^{LMMSE}, f_{j,1}^{LPCA}, f_{j,2}^{LPCA}, f_{j,3}^{LPCA}\right]^T \tag{12}$$

where $f_{j,1}^{LMMSE}$, $f_{j,2}^{LMMSE}$, $f_{j,3}^{LMMSE}$, $f_{j,1}^{LPCA}$, $f_{j,2}^{LPCA}$ and $f_{j,3}^{LPCA}$ are the summed image intensity values at pixel j, obtained from $[S^{LMMSE}(b_2) + S^{LMMSE}(b_3) + S^{LMMSE}(b_4)]$, $[S^{LMMSE}(b_5) + S^{LMMSE}(b_6) + S^{LMMSE}(b_7)]$, $[S^{LMMSE}(b_8) + S^{LMMSE}(b_9) + S^{LMMSE}(b_{10})]$, $[S^{LPCA}(b_2) + S^{LPCA}(b_3) + S^{LPCA}(b_4)]$, $[S^{LPCA}(b_5) + S^{LPCA}(b_6) + S^{LPCA}(b_7)]$, and $[S^{LPCA}(b_8) + S^{LPCA}(b_9) + S^{LPCA}(b_{10})]$, respectively. $S^{LMMSE}(b_i)$ and $S^{LPCA}(b_i)$ are the ith b-value DW-MRI signal intensities denoised by the LMMSE method and the LPCA method, respectively. All the other settings used in the construction of the kernel matrix remained the same. This denoising method was be referred to as the smoothed kernel (SKernel). The denoising method used noisy DW-MRI data to construct the kernel matrix was be referred to as the Kernel. We compared the proposed method with the LPCA method (Manjón et al., 2013). The LPCA method is chosen because it can take into account the four-dimensional nature of DW-MRI dataset. In addition, the LPCA method integrates an automatic noise estimation method, and there is no requirement to define input parameters. One recent study showed that the LPCA method outperforms several image denoising methods including the original nonlocal means algorithm and its variant (Reischauer and Gutzeit, 2017).

2.2. IVIM analysis

IVIM parameters derived from DW-MRI data have many clinical applications (Freiman et al., 2013; Kang et al., 2014; Luciani et al., 2008; Sigmund et al., 2012), but their applications are often hindered due to poor image quality (Koh et al., 2011). Here, we focus on investigating whether DW-MRI data denoised using the proposed method can improve IVIM parametric images. In general, the IVIM model assumes a biexponential function that describes the DW-MRI signal decay as a function of diffusion sensitivity (i.e. b-value) (LeBihan et al., 1988, 1986):

$$S(b) = S_o\left[(1 - PF) \times e^{-b \times D} + PF \times e^{-b \times D^*}\right] \tag{13}$$

S_o and $S(b)$ denote the DW-MRI signal intensities obtained by b-values of 0 and b s/mm^2, respectively. Perfusion fraction (PF), diffusion coefficient (D) and pseudodiffusion coefficient (D^*) are IVIM model parameters to be estimated. In the present work, pixel-wise IVIM analysis was performed based on a segmented-unconstrained method (Pekar et al., 1992). The segmented-unconstrained fit method assumes that D^* is much larger than D. Thus, the Eq. (13) can be simplified to:

$$S(b) \approx S_o\left[(1 - PF) \times e^{-b \times D}\right] \tag{14}$$

The model parameters PF and D can be estimated by fitting the Eq. (14) to the DW-MRI data with $b \geq 200$ s/mm^2. Then, the parameter D^* can be estimated by fixing PF and D at the value estimated above and fitting the Eq. (13) to the DW-MRI data with $b \geq 0$ s/mm^2. The estimation of IVIM parameters was determined by the trust-region-reflective least squares algorithm (Branch et al., 1999; Byrd et al., 1988) which can be implemented via Matlab's lsqcurvefit function. Initial values for PF, D and D^* were set to 0.01, 0.002 mm^2/s and 0.05 mm^2/s, respectively. The lower and upper bounds were set as $0 \leq PF \leq 1$, $0 \leq D \leq 0.003$ mm^2/s and $0 \leq D^* \leq 0.2$ mm^2/s.

2.3. Simulation parameters and performance evaluation

In this work, we used a digital phantom which simulated four lesions: liver, pancreas, spleen and kidney. We also simulated lesions of different sizes (3, 5 and 7 pixels in radius). The parameter PF for background, liver, pancreas, spleen and kidney was set to 0.1, 0.31, 0.248, 0.13 and 0.187, respectively (Freiman et al., 2013; Kang et al., 2014; Luciani et al., 2008; Sigmund et al., 2012). The parameter D for background, liver, pancreas, spleen and kidney was set to 0.4×10^{-3}, 1.0×10^{-3}, 1.2×10^{-3}, 0.75×10^{-3} and 2.0×10^{-3} mm^2/s, respectively (Freiman et al., 2013; Kang et al., 2014; Luciani et al., 2008; Sigmund et al., 2012). The parameter D^* for background, liver, pancreas, spleen and kidney was set to 15×10^{-3}, 71×10^{-3}, 36×10^{-3}, 30×10^{-3} and 24.5×10^{-3} mm^2/s, respectively (Freiman et al., 2013; Kang et al., 2014; Luciani et al., 2008; Sigmund et al., 2012). Based on Eq. (13), noise-free DW-MR magnitude images ($S_o = 400$) were computed with b-values of 0 (b_1), 10 (b_2), 20 (b_3), 30 (b_4), 50 (b_5), 80 (b_6), 100 (b_7), 200 (b_8), 400 (b_9) and 800 (b_{10}) s/mm^2. The noise-free DW-MR magnitude image was corrupted with five different levels of Rician noise (i.e. $SNR_{b=0}$: 10, 20, 30, 40 and 50). Computer simulation was repeated fifty times at each level of Rician noise.

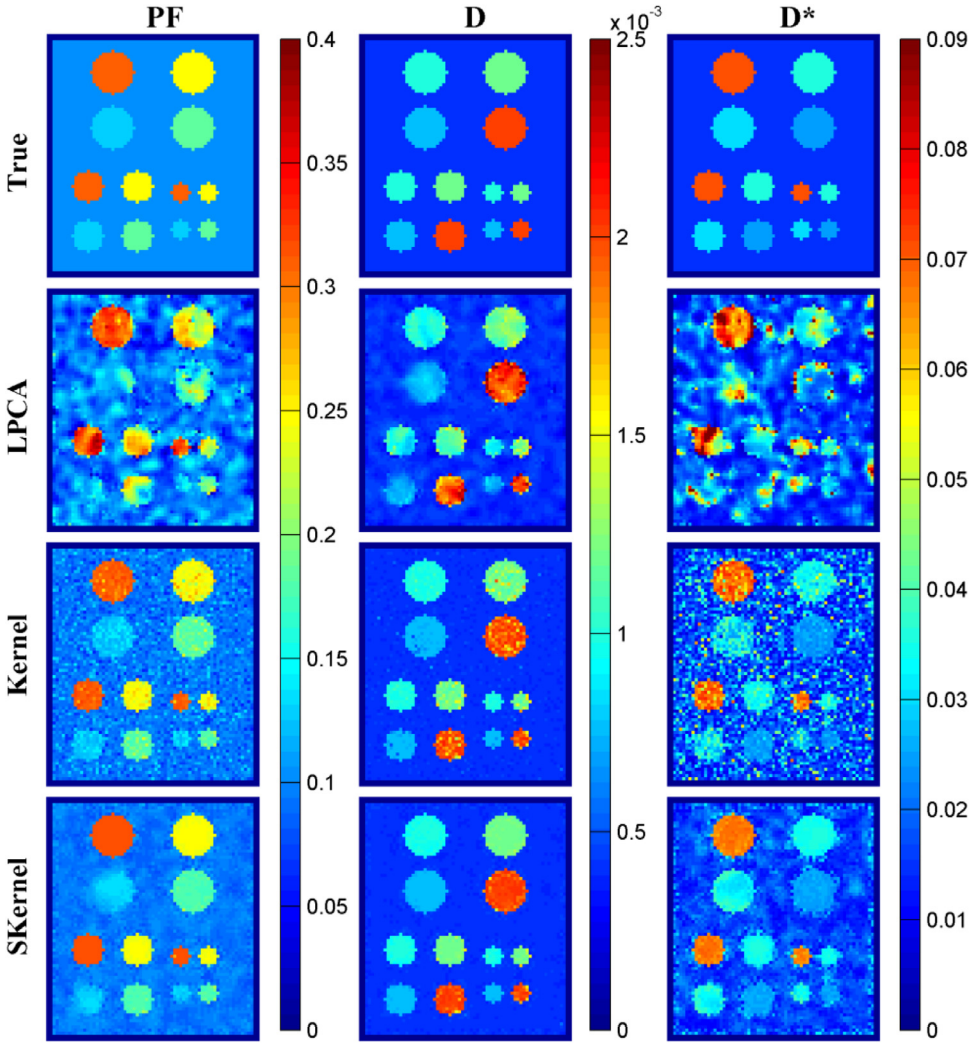

Fig. 1. Parameter maps of PF, D, and D* (rows) obtained using different image denoising methods (columns), compared with the true values (top row), for the simulated data SNR of 20.

For quantitative comparison between different denoising methods, we computed the bias, coefficient of variation (CV) and root-mean-square error (RMSE), which are defined as follows:

$$\text{Bias} = \frac{1}{T}\sum_{t\in L}\frac{\left[\frac{1}{S}\left(\sum_{s=1}^{S} P_{st}^{est}\right) - P_t^{true}\right]}{P_t^{true}} \tag{15}$$

$$\text{CV} = \frac{1}{T}\sum_{t\in L}\frac{\sigma_t}{\frac{1}{S}\sum_{s=1}^{S} P_{st}^{est}} \tag{16}$$

$$\text{RMSE} = \sqrt{\frac{\sum_{t\in L}\sum_{s=1}^{S}\left(P_{st}^{est} - P_t^{true}\right)^2}{S\times T}} \tag{17}$$

where P_{st}^{est} is the estimated parametric image for the tth pixel of the sth noise realization, P_t^{true} is the true parametric image for the tth pixel, σ_s is the SD of the IVIM parameter estimate for the tth pixel across all noise realizations, S is the number of noise realizations, and T is the number of pixels in the lesion. The RMSE, bias and CV were calculated separately for each lesion, and the mean values over four lesions were presented.

2.4. Patient study and MRI protocols

We tested the proposed method on five patients with Hodgkin lymphoma. This study was approved by the institutional review board of Chang Gung Memorial Hospital, and the patients gave informed consent. DW-MRI data with 10 b values (i.e. 0, 10, 20, 30, 50, 80, 100, 200, 400, and 800 s/mm^2) were acquired in the axial plane during free breathing on a 3 T hybrid PET/MR system (Biograph mMR, Siemens Healthcare, Erlangen, Germany). A prototype single-shot twice-refocused spin-echo sequence with the following acquisition parameters was used: monopolar diffusion gradients, axial echo-planar imaging readout, repetition time: 6100 ms, echo time: 59 ms, field of view: 320 × 256 mm^2, matrix size: 130 × 104, slice thickness: 5 mm, number of slice: 30, number of excitation: 3, receiver bandwidth: 2404 Hz per pixel, and generalized autocalibrating partially parallel acquisition factor of two.

3. Results

Fig. 1 shows the estimated IVIM parametric images obtained using different image denoising methods for a single noise realization with $SNR_{b=0}$ of 20. It is clear that the two kernel-based methods substantially improved the parametric image quality over the LPCA method for all three IVIM parameters. Moreover, compared to the Kernel method, the SKernel method can suppress noise more effectively, with only slight loss of spatial information. Fig. 2 shows the bias, CV and RMSE of the different image denoising methods as a function of noise levels (i.e. $SNR_{b=0}$). Overall, the two kernel-based methods outperform the LPCA method in terms of RMSE. In

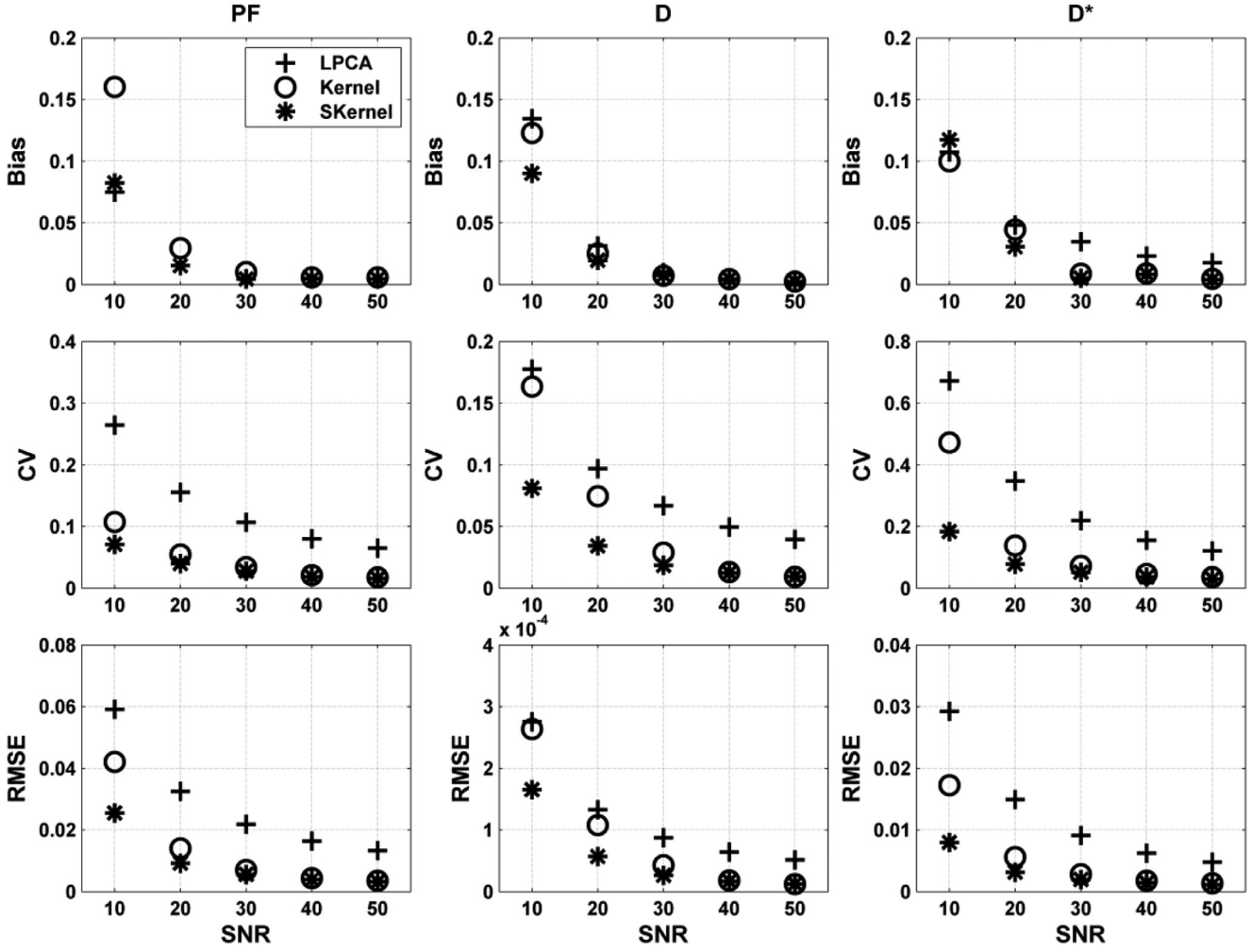

Fig. 2. Bias (top row), CV (middle row) and RMSE (bottom row) of PF (left column), D (middle column), and D* (right column), averaged over four lesions for each image denoising method at five different SNR levels.

addition, the proposed kernel-based methods show a great improvement over the LPCA method in CV. When $SNR_{b=0} > 10$, the proposed SKernel method can reduce bias in parameter estimates of D*. It can be observed that when $SNR_{b=0} < 30$, the Kernel method shows a modest improvement over the LPCA method. This indicates that the kernel matrix constructed by noisier data can affect the performance of the kernel-based denoising method. This is why we propose the SKernel method that constructs the kernel matrix using the smoothed data.

As illustrated in Fig. 3, we applied the proposed SKernel method to a DW-MRI scan of a real patient. The results obtained from the Kernel method were not shown because the estimated $SNR_{b=0}$ was approximately 27 which suggested using the SKernel method. It is not surprising that the LPCA method can produce high-quality parametric images than the method without using image denoising (i.e. No filter). However, the LPCA method still tends to either over or underestimate the values of PF and D*. For example, in one patient's ROI, the LPCA method yielded many parameter estimates (17% for PF and 16% for D*) that fell outside the reasonable range (i.e. PF < 0.01 or >0.5 and D* < 0.001 or >0.1 mm^2/s). In contrast, the proposed SKernel method didn't overestimate or underestimate the values of PF and D*. Tables 1 and 2 summarize the IVIM parameter estimates for all patients, and Fig. 4 illustrates the ROI placement in a patient. The mean IVIM parameter values obtained from both the proposed SKernel method and the LPCA method were similar. However, the proposed SKernel method had smaller CV (i.e. the ratio of the SD to the mean) than the LPCA method, especially for the D* parameter.

Finally, we assessed the runtime of each image denoising method on a desktop computer equipped with a 3.0 GHz Intel i7-5960 processor with 64 GB of RAM. The runtime to denoise one DW-MRI data set (i.e. matrix: $104 \times 130 \times 30 \times 10$) using the SKernel method and the LPCA method was approximately 194.3 and 6.6 s, respectively. Due to the thresholding operator (i.e. Eq. (7)), the SKernel method took approximately thirty times longer than the LPCA method to perform image denoising. However, we could use either multi-core processor or graphics processing unit to reduce the runtime of the proposed SKernel method.

4. Discussion

In this study, we proposed a kernel-based method to solve the problem of image denoising. We examined whether the DW-MRI data after denoising using the proposed method can provide improved IVIM parametric images. Simulation results showed that the proposed method yielded more reliable IVIM parametric images than the LPCA method, especially for PF and D* (Figs. 1 and 2). Our experimental results showed that both PF and D* parameters were either over- or under-estimated by the LPCA method. As a result, the LPCA method had poor precision (i.e. high CV). In

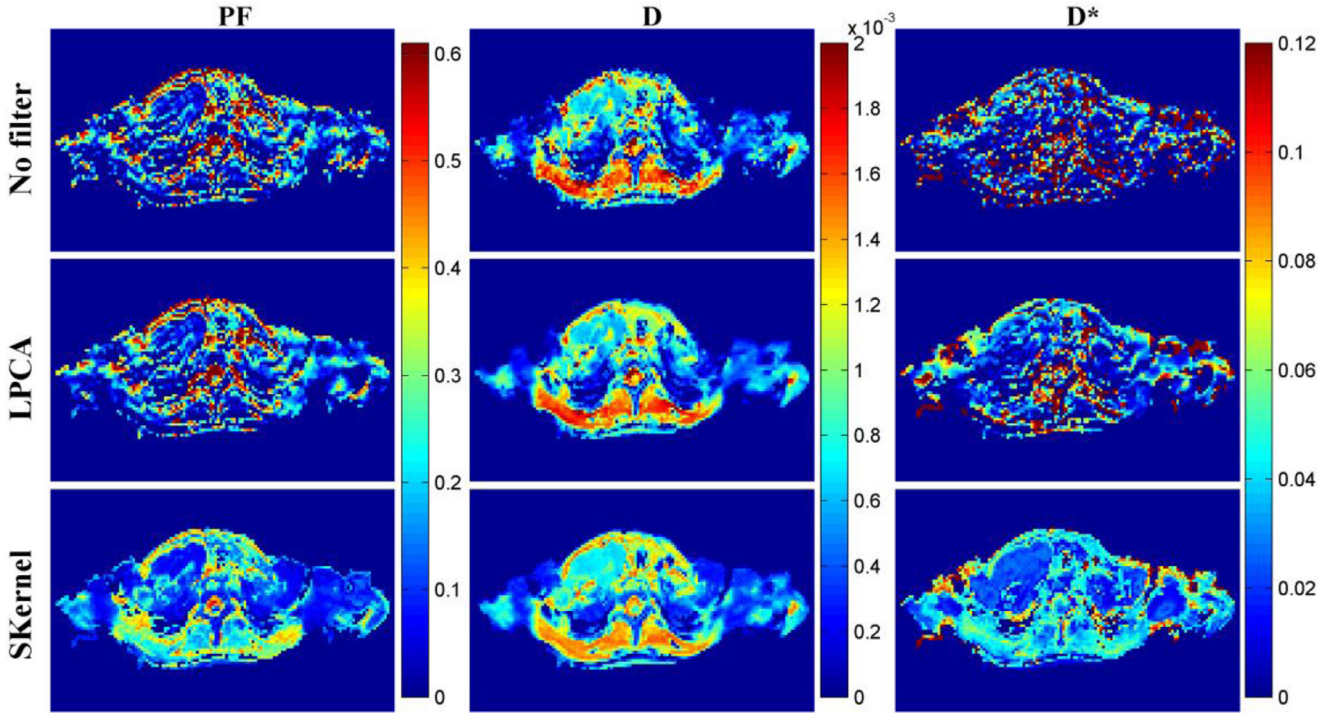

Fig. 3. Parametric images of PF, D, and D* (columns) of the real patient data obtained from noisy data (top row) and denoised data using the LPCA method (middle rows) and the SKernel method (bottom rows).

Table 1
Values of IVIM Parameters (mean ± SD) obtained from patient DW-MRI data denoised using the LPCA method and the SKernel method.

Patients	LPCA			SKernel		
	PF (no unit)	D ($\times 10^{-3}$ mm^2/s)	D* ($\times 10^{-3}$ mm^2/s)	PF (no unit)	D ($\times 10^{-3}$ mm^2/s)	D* ($\times 10^{-3}$ mm^2/s)
1	0.095 ± 0.037	1.00 ± 0.26	43.4 ± 40.2	0.119 ± 0.045	0.97 ± 0.19	17.4 ± 2.6
2	0.074 ± 0.059	0.69 ± 0.13	21.3 ± 15.6	0.077 ± 0.015	0.70 ± 0.04	24.9 ± 2.4
3	0.061 ± 0.033	0.71 ± 0.13	22.3 ± 14.4	0.102 ± 0.025	0.80 ± 0.10	18.5 ± 6.0
4	0.054 ± 0.049	1.40 ± 0.18	32.4 ± 34.6	0.086 ± 0.013	1.39 ± 0.04	14.9 ± 2.1
5	0.112 ± 0.037	0.99 ± 0.10	31.2 ± 14.5	0.092 ± 0.019	1.01 ± 0.11	40.4 ± 9.8
Mean ± SD	0.079 ± 0.024	0.96 ± 0.29	30.0 ± 8.9	0.095 ± 0.016	0.97 ± 0.26	23.2 ± 10.3

Table 2
CV of estimated IVIM parameters obtained from patient DW-MRI data denoised using the LPCA method and the SKernel method.

Patients	LPCA			SKernel		
	PF	D	D*	PF	D	D*
1	0.39	0.26	0.93	0.37	0.20	0.15
2	0.80	0.18	0.73	0.20	0.05	0.10
3	0.54	0.19	0.65	0.24	0.13	0.32
4	0.90	0.13	1.07	0.15	0.03	0.14
5	0.33	0.10	0.46	0.20	0.11	0.24

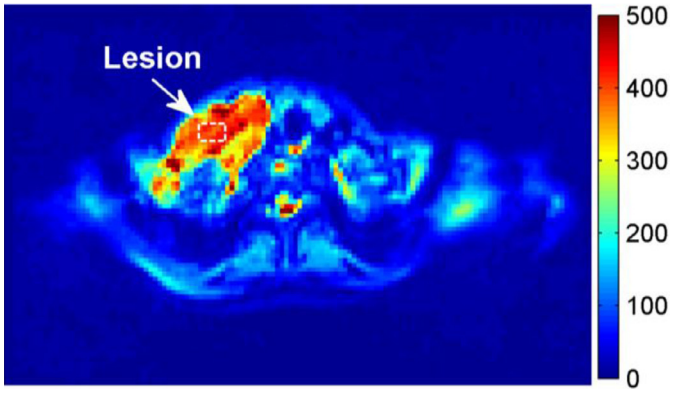

Fig. 4. DW-MRI image with b-value=50 s/mm^2. The white arrow indicates the lesion and a ROI was drawn manually (white dashed line).

contrast, the proposed method yielded precise IVIM parameter estimates (Tables 1 and 2). These results indicate that the proposed method can increase the reliability of quantitative analysis of DW-MRI data.

The kernel-based method implemented in this study and previous studies (Wang and Qi, 2015; Gong et al., 2018) is different from other methods such as non-local means (Dutta et al., 2013) and bilater filter (Bian et al., 2014). Although these methods make use of similarity information and of the radial Gaussian kernel, they assume that a target pixel is calculated as a weighted average of its neighbors. The weighting factors are determined by noisy neighboring pixels. In contrast, the kernel-based method assumes that the PET image intensity can be modeled as a linear function in the kernel space (Wang and Qi, 2015). The prior images used to construct the kernel (i.e. weighting) matrix consist of denoised

data (i.e. Eq. (12)) which can provide appropriate weighting factors. Moreover, the kernel-based method used a knn search which could find similar neighbors.

The proposed kernel-based image denoising method, like most image denoising methods, has several algorithm parameters such as λ, p, n, σ, the number of neighbors and thresholding operations. Except for λ which was determined automatically, other parameters were predefined. Despite most algorithm parameters being fixed, the proposed method can provide improved results for different SNR levels. This indicates that most algorithm parameters are less sensitive to noise. Based on our preliminary tests (not shown), we also observed that the performance of the proposed method can be slightly improved by fine-tuning algorithm parameters.

Our results show that the SKernel method can improve the parametric image quality even if prior images are obtained from low-SNR (i.e. $SNR_{b=0} < 30$) DW-MRI data. To further improve the performance of the proposed method, several strategies can be implemented. First, the image denoising methods (i.e. LMMSE and LPCA) used to generate smoothed prior images can be replaced by other advanced smoothing techniques (Manjón et al., 2012). Second, we can use advanced curve fitting algorithms (Freiman et al., 2013; Guo et al., 2009; Kayal et al., 2017; Lin et al., 2017; Orton et al., 2014) to estimate IVIM parameters, though the computation time may increase dramatically. Third, we can extend the construction of the kernel matrix to three-dimensional cases.

Although it is possible to further improve the performance of the proposed method, there are some issues that need to be addressed. First, DW-MRI data with 9 different b-values were used to construct the kernel matrix. The kernel matrix would be affected by reducing the number of b-values or changing the combination of b-values. Second, organ motion (Veraart et al., 2013) that leads to mismatches between the prior images and the undenoised images can affect the performance of the proposed method. These issues suggest that optimization of b-value and motion correction are required in order to provide reliable parametric images.

5. Conclusion

In this paper, we proposed a kernel-based method for image denoising. We used the GTF algorithm in combination with TD to solve the kernelized image denoising problem. We applied the proposed kernel-based method for denoising DW-MRI data, and results on both simulated and real DW-MRI data demonstrated that the proposed image denoising method can provide higher-quality parametric images than the LPCA method, especially in the case of high noise levels (i.e. $SNR_{b=0} < 30$).

Acknowledgments

This work was supported by MOST 107-2221-E-002-081, 107-2314-B-182A-121 and 106-2314-B-182A-020 from Ministry of Science Technology, Taiwan, and CMRPG392043, CMRPG3F1131, CMRPG3F1132, and NSC101-2923-B-182A-001-MY3 from the Research Fund of Chang Gung Memorial Hospital, Taiwan. The authors would like to thank Dr. Thorsten Feiweier from Siemens Healthcare for providing the prototype sequence used in this work.

Conflict of interest

All authors declare that they have no conflicts of interest. All authors have approved the manuscript for submission. The content of the manuscript has not been published, or submitted for publication elsewhere.

Appendix

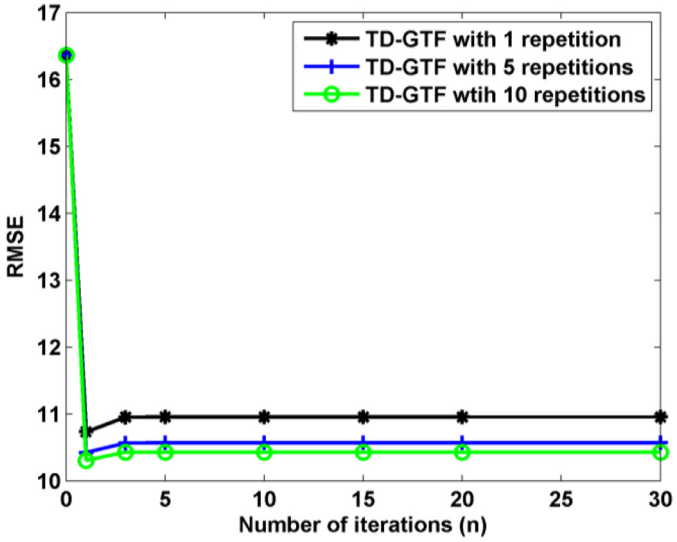

Fig. A1. RMSE versus the number of iterations (n). The RMSE between the true and denoised DW-MRI data was calculated. The simulated DW-MRI data ($SNR_{b=0} = 30$) were denoised using the proposed method. In the proposed method, the filtering process (i.e. TD-GTF) was repeated several times. We found that the TD-GTF method with 5 repetitions was similar to that with 10 repetitions. Therefore, the TD-GTF method with 5 repetitions was used. After 5 iterations, the proposed method can achieve stable results. n was set to 10 in order to deal with high levels of noise.

References

Aja-Fernandez, S., Niethammer, M., Kubicki, M., Shenton, M.E., Westin, C.-F., 2008. Restoration of DWI data using a Rician LMMSE estimator. IEEE Trans. Med. Imaging 27 (10), 1389–1403.

Branch, M.A., Coleman, T.F., Li, Y., 1999. A subspace, interior, and conjugate gradient method for large-scale bound-constrained minimization problems. SIAM J. Sci. Comput. 21 (1), 1–23.

Bian, Z., Huang, J., Ma, J., Lu, L., Niu, S., Zeng, D., Feng, Q., Chen, W., 2014. Dynamic positron emission tomography image restoration via a kinetics-induced bilateral filter. PLoS One 9 (2), e89282.

Byrd, R.H., Schnabel, R.B., Shultz, G.A., 1988. Approximate solution of the trust region problem by minimization over two-dimensional subspaces. Math. Program. 40 (1–3), 247–263.

Coupé, P., Manjón, J.V., Gedamu, E., Arnold, D., Robles, M., Collins, D.L., 2010. Robust Rician noise estimation for MR images. Med. Image Anal. 14 (4), 483–493.

Dutta, J., Leahy, R.M., Li, Q., 2013. Non-local means denoising of dynamic PET images. PLoS One 8 (12), e81390.

Fessler, J.A., 2010. Model-based image reconstruction for MRI. IEEE Signal Process. Mag. 27 (4), 81–89.

Freiman, M., Perez-Rossello, J.M., Callahan, M.J., Voss, S.D., Ecklund, K., Mulkern, R.V, Warfield, S.K., 2013. Reliable estimation of incoherent motion parametric maps from diffusion-weighted MRI using fusion bootstrap moves. Med. Image Anal. 17 (3), 325–336.

Geyer, L.L., Schoepf, U.J., Meinel, F.G., Nance, J.W., Bastarrika, G., Leipsic, J.A., Paul, N.S., Rengo, M., Laghi, A., DeCecco, C.N., 2015. State of the art: iterative CT reconstruction techniques. Radiology 276 (2), 339–357.

Gong, K., Cheng-Liao, J., Wang, G., Chen, K.T., Catana, C., Qi, J., 2018. Direct Patlak reconstruction from dynamic PET data using the Kernel method with MRI information based on structural similarity. IEEE Trans. Med. Imaging 37 (4), 955–965.

Gudbjartsson, H., Patz, S., 1995. The Rician distribution of noisy MRI data. Magn. Reson. Med. 34 (6), 910–914.

Guo, H., Renaut, R.A., Chen, K., Reiman, E., 2009. FDG-PET parametric imaging by total variation minimization. Comput. Med. Imaging Gr. 33 (4), 295–303.

Hofmann, T., Scholkopf, B., Smola, A.J., 2008. Kernel methods in machine learning. Ann. Stat. 36 (3), 1171–1220.

Kang, K.M., Lee, J.M., Yoon, J.H., Kiefer, B., Han, J.K., Choi, B.I., 2014. Intravoxel incoherent motion diffusion-weighted MR imaging for characterization of focal pancreatic lesions. Radiology 270 (2), 444–453.

Kayal, E.B., Kandasamy, D., Khare, K., Alampally, J.T., Bakhshi, S., Sharma, R., Mehndiratta, A., 2017. Quantitative analysis of intravoxel incoherent motion (IVIM) diffusion MRI using total variation and Huber penalty function. Med. Phys. 44 (11), 5849–5858.

Khalifa, F., Soliman, A., El-Baz, A., Abou El-Ghar, M., El-Diasty, T., Gimel'farb, G., Ouseph, R., Dwyer, A.C., 2014. Models and methods for analyzing DCE-MRI: a review. Med. Phys. 41 (12), 124301.

Koh, D.-M., Collins, D.J., Orton, M.R., 2011. Intravoxel incoherent motion in body diffusion-weighted MRI: reality and challenges. Am. J. Roentgenol. 196 (6), 1351–1361.

LeBihan, D., Breton, E., Lallemand, D., Aubin, M.L., Vignaud, J., Laval-Jeantet, M., 1988. Separation of diffusion and perfusion in intravoxel incoherent motion MR imaging. Radiology 168 (2), 497–505.

LeBihan, D., Breton, E., Lallemand, D., Grenier, P., Cabanis, E., Laval-Jeantet, M., 1986. MR imaging of intravoxel incoherent motions: application to diffusion and perfusion in neurologic disorders. Radiology 161 (2), 401–407.

Levenberg, K., 1944. A method for the solution of certain problems in least squares. Q. Appl. Math. 2, 164–168.

Lin, C., Liu, C.-C., Huang, H.-M., 2018. A general-threshold filtering method for improving intravoxel incoherent motion parameter estimates. Phys. Med. Biol. 63 (17), 175008.

Lin, C., Shih, Y.-Y., Huang, S.-L., Huang, H.-M., 2017. Total variation-based method for generation of intravoxel incoherent motion parametric images in MRI. Magn. Reson. Med. 78 (4), 1383–1391.

Luciani, A., Vignaud, A., Cavet, M., Nhieu, J.T.Van, Mallat, A., Ruel, L., Laurent, A., Deux, J.-F., Brugieres, P., Rahmouni, A., 2008. Liver cirrhosis: intravoxel incoherent motion MR imaging–pilot study. Radiology 249 (3), 891–899.

Manjón, J.V., Coupé, P., Buades, A., Louis Collins, D., Robles, M., 2012. New methods for MRI denoising based on sparseness and self-similarity. Med. Image Anal. 16 (1), 18–27.

Manjón, J.V, Coupé, P., Concha, L., Buades, A., Collins, D.L., Robles, M., 2013. Diffusion weighted image denoising using overcomplete local PCA. PLoS One 8 (9), e73021.

Marquardt, D.W., 1963. An algorithm for least-squares estimation of nonlinear parameters. J. Soc. Ind. Appl. Math. 11 (2), 431–441.

Miao, C., Yu, H., 2015. A general-thresholding solution for ℓp ($0 < p < 1$) regularized CT reconstruction. IEEE Trans. Image Process. 24 (12), 5455–5468.

Milanfar, P., 2013. Symmetrizing Smoothing Filters. SIAM J. Imaging Sci. 6 (1), 263–284.

Muzi, M., O'Sullivan, F., Mankoff, D.A., Doot, R.K., Pierce, L.A., Kurland, B.F., Linden, H.M., Kinahan, P.E., 2012. Quantitative assessment of dynamic PET imaging data in cancer imaging. Magn. Reson. Imaging 30 (9), 1203–1215.

Orton, M.R., Collins, D.J., Koh, D.-M., Leach, M.O., 2014. Improved intravoxel incoherent motion analysis of diffusion weighted imaging by data driven Bayesian modeling. Magn. Reson. Med. 71 (1), 411–420.

Pekar, J., Moonen, C.T., vanZijl, P.C., 1992. On the precision of diffusion/perfusion imaging by gradient sensitization. Magn. Reson. Med. 23 (1), 122–129.

Reischauer, C., Gutzeit, A., 2017. Image denoising substantially improves accuracy and precision of intravoxel incoherent motion parameter estimates. PLoS One 12 (4), e0175106.

Sigmund, E.E., Vivier, P.-H., Sui, D., Lamparello, N.A., Tantillo, K., Mikheev, A., Rusinek, H., Babb, J.S., Storey, P., Lee, V.S., Chandarana, H., 2012. Intravoxel incoherent motion and diffusion-tensor imaging in renal tissue under hydration and furosemide flow challenges. Radiology 263 (3), 758–769.

Sijbers, J., den Dekker, A.J., Scheunders, P., Van Dyck, D., 1998. Maximum-likelihood estimation of Rician distribution parameters. IEEE Trans. Med. Imaging 17 (3), 357–361.

Schölkopf, B., Smola, A.J., 2001. Learning with Kernels: Support Vector Machines, Regularization, Optimization, and Beyond.

Tong, S., Alessio, A.M., Kinahan, P.E., 2010. Image reconstruction for PET/CT scanners: past achievements and future challenges. Imaging Med. 2 (5), 529–545.

Valdiviezo, C., Ambrose, M., Mehra, V., Lardo, A.C., Lima, J.A.C., George, R.T., 2010. Quantitative and qualitative analysis and interpretation of CT perfusion imaging. J. Nucl. Cardiol. 17 (6), 1091–1100.

Veraart, J., Rajan, J., Peeters, R.R., Leemans, A., Sunaert, S., Sijbers, J., 2013. Comprehensive framework for accurate diffusion MRI parameter estimation. Magn. Reson. Med. 70 (4), 972–984.

Wang, G., Qi, J., 2009. Generalized algorithms for direct reconstruction of parametric images from dynamic PET data. IEEE Trans. Med. Imaging 28 (11), 1717–1726.

Wang, G., Qi, J., 2015. PET image reconstruction using kernel method. IEEE Trans. Med. Imaging 34 (1), 61–71.

Yu, H., Wang, G., 2010. A soft-threshold filtering approach for reconstruction from a limited number of projections. Phys. Med. Biol. 55 (13), 3905–3916.